THE JOURNAL OF PHYSICAL CHEMISTRY B

Article

pubs.acs.org/JPCB

Adsorption of Glucose, Cellobiose, and Cellotetraose onto Cellulose Model Surfaces

Johannes Hoja,[†] Reinhard J. Maurer,[‡] and Alexander F. Sax*[,†]

[†]Department of Chemistry, University of Graz, 8010 Graz, Austria

[‡]Department Chemie, Technische Universität München, 85748 Garching, Germany

Supporting Information

ABSTRACT: Reliable simulation of molecular adsorption onto cellulose surfaces is essential for the design of new cellulose nanocomposite materials. However, the applicability of classical force field methods to such systems remains relatively unexplored. In this study, we present the adsorption of glucose, cellobiose, and cellotetraose on model surfaces of crystalline cellulose Iα and Iβ. The adsorption of the two large carbohydrates was simulated with the GLYCAM06 force field. To validate this approach, quantum theoretical calculations for the adsorption of glucose were performed: Equilibrium geometries were studied with density functional theory (DFT) and dispersion-corrected DFT, whereas the adsorption energies were calculated with two standard density functional approximations and five dispersion-containing DFT approaches. We find that GLYCAM06 gives a good account of geometries and, in most cases, accurate adsorption energies when compared to dispersion-corrected DFT energies. Adsorption onto the (100) surface of cellulose Iα is, in general, stronger than onto the (100) surface of cellulose Iβ. Contrary to intuition, the adsorption energy is not directly correlated with the number of hydrogen bonds; rather, it is dominated by dispersion interactions. Especially for bigger adsorbates, a neglect of these interactions leads to a dramatic underestimation of adsorption energies.

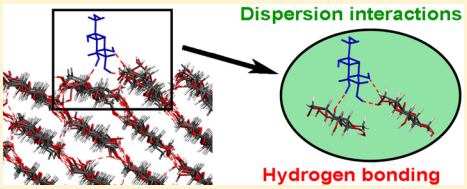

INTRODUCTION

The organic polymer, cellulose, is the main constituent of plants, and therefore one of the most abundant materials on earth.[1] Due to its propensity for adhesion and self-adhesion, cellulose is also a useful component in fiber-based composite materials, especially nanocomposites. Cellulose nanocomposites show very different chemical properties from larger cellulose components. These nanocomposites can be used, for example, in transparent films,[2] textiles,[3] flexible displays,[4] and barrier films.[5] In all of these examples, the stability and functionality of the material critically depend on the interactions of the different composites, whereby the known amphiphilic character of cellulose[6] offers a great variety of interactions. The origin of the amphiphilic character lies in the molecular structure of the glucopyranose ring: its equatorial direction has a hydrophilic character because all three hydroxyl groups are located on the equatorial positions of the ring, whereas all hydrogen atoms of the CH groups are located in the axial position.[7] This structural anisotropy of the glucose ring and the possibility to form intrachain hydrogen bonds in a glucan molecule is responsible for the amphiphilic character of the ribbon-like glucan molecules. When glucan molecules are parallel arranged with their hydrophilic edges side by side, interchain hydrogen bonds can be formed between them and the sheets formed in this way are dominantly hydrophobic. Stacks of glucan ribbons are held together by the so-called hydrophobic interaction; top and bottom faces of such a stack are hydrophobic but the side faces are hydrophilic. This view is compatible with the experimental finding that native cellulose I[8,9] consists of sheets composed of parallel-aligned glucan molecules. The traditional explanation of the stability of crystalline cellulose is that the only attractive interaction between glucan molecules within a sheet is hydrogen bonding and that the sheets themselves are held together by weak van der Waals interactions,[10] although weak C−H···O hydrogen bonds have also been proposed to account for the intersheet attractions.[11,12] In contrast to this traditional explanation, Lindman and co-workers[6,7,13] claim that hydrophobic interactions are more important than hydrogen bonding and, therefore, are responsible for the stability of cellulose and for its bad solubility in polar solvents. It is not necessary to find solvents that allow us to break the hydrogen bonds, which are allegedly responsible for the bad solubility of cellulose,[14,15] when hydrophobic interactions are responsible for the stability. This is the basis of the so-called *Lindman hypothesis*:[16] "Insolubility of cellulose comes from its hydrophobicity". Recently, Isobe et al.[17] and Xiong et al.[18] suggested an explanation of the role of urea in ionic solvents for cellulose using the Lindman hypothesis. According to them, the solubilized fraction of microcrystalline cellulose in an alkali/urea system is stabilized by preventing hydrophobic mutual association of cellulose. But also for adsorption, hydrophobic interactions are important. Because facets of microcrystallites can be regarded as finite subsets of crystal planes, they have the

Received: March 14, 2014
Revised: May 26, 2014
Published: July 2, 2014

   dx.doi.org/10.1021/jp5025685 | J. Phys. Chem. B 2014, 118, 9017−9027

same properties as the latter. Therefore, if a facet of a cellulose microfibril is formed by a sheet of glucan molecules, it is as hydrophobic as the sheet itself. All crystal surfaces cutting through the parallel sheets are strongly structured, having more or less deep grooves separated by ridges with protruding hydroxyl groups. Such surfaces show, therefore, hydrophilicity of various degrees. The rough (110) surface in cellulose Iβ, for example, is hydrophilic but the flat (100) surface is hydrophobic. This is responsible for the different wettability of the two surfaces.[19] The hydrophobic (100) surface is also very important in nature, because cellulases adsorb initially only at this surface.[20]

The adsorption of carbohydrates onto cellulose surfaces is governed by noncovalent interactions, which can be partitioned into four components.[21] The first component covers the interactions between permanent multipoles (electrostatics), the second the interaction between permanent and induced multipoles (induction), and the third the interaction between multipoles—which are instantaneously created in the electron cloud of an atom—and induced multipoles in the electron cloud of another atom (dispersion). The electrostatic interaction is anisotropic, whereas the dispersion interaction is held as largely isotropic and increasing with the number of atoms in close contact. The fourth interaction component is the short-range repulsive interaction between electrons with like spins, which is frequently termed the exchange or Pauli repulsion. The term *van der Waals interaction* is sometimes used to describe the sum of attractive dispersion and repulsive exchange, mainly motivated by the form of the Lennard-Jones potential; sometimes it is used as a synonym for the attractive dispersion only. We prefer the latter use. According to the standard classification of noncovalent interactions, *hydrophobic interaction* should be a synonym with *van der Waals interaction*. The term *hydrogen bonding* is used to describe traditionally a special kind of noncovalent interaction between two molecules caused by a characteristic moiety, D−H···A, with a polar D−H donor group and an electronegative acceptor atom A. In cellulose, this moiety is always the O−H···O atom group, which, according to Jeffrey's classification,[22] belongs to moderate hydrogen bonding. The interaction between a C−H bond and oxygen atoms has also been called *weak hydrogen bonding*.[9] In this paper, we will use the term hydrogen bond to represent only moderate hydrogen bonds. Hydrogen bonding is frequently attributed to dominant electrostatic interactions between the donor group and the acceptor atom; however, noncovalent interactions always consist of the four components described above. Even in the water dimer, about 50% of the interaction energy is due to dispersion interaction, as we showed in a recent study on alcohol dimers.[23] In this study, we showed also that the importance of the dispersion component increases with the size and bulk of the molecules, because the number of atoms in close contact also increases with size. In the *tert*-butanol dimer, the dispersion interaction is responsible for about 90% of the dimer stabilization energy at the equilibrium geometry, with the sum of electrostatic, induction, and exchange interactions amounting to only 10%. This would not be the case, if indeed the O−H···O atom groups were solely responsible for hydrogen bonding. Because every glucose ring can be seen as a large, bulky substituent of its OH groups, a large part of the attraction of glucan chains in a sheet will be due to dispersion, without neglecting the electrostatic contributions to interchain hydrogen bonding.

What is said about the bonding interactions in bulk cellulose also holds for adsorption onto cellulose surfaces: the larger the adsorbate is, the more atoms will be in close contact and the larger is the dispersion interaction. Additional surface OH groups (hydrophilic surface) will give additional attractive electrostatic interactions. The ratio of dispersion and non-dispersive interaction will depend on the size of the adsorbate, and on the methods used to describe the interactions. Several adsorption studies in the literature differ in the type of adsorbates and the theoretical level of the methods; in some studies water as solvent is explicitly included, but many studies describe adsorption in the gas phase. With molecular dynamics methods adsorption energies are indeed free energy differences accounting for entropic effects, such as conformational entropy of the adsorbate or the entropy differences between adsorbed, immobilized water and bulk water with its large entropy contributions.

Adsorption of carbohydrates was investigated by several groups,[24−28] adsorbates with aromatic rings were investigated in the group of Mazeau,[29,30] adsorption of small proteins on cellulose was investigated by Nimlos et al.,[31] and adsorption of inorganic nanoparticles on cellulose nanofibrils was investigated by Nypelö et al.[32] Because in many experiments adsorption from solution is investigated, good arguments must be given to justify adsorption without explicit accounting for solvent effects. Mazeau and Charlier[26] claim that such modeling setups mimic "bad solvent conditions", leading to an overestimation of the interaction energies of a magnitude that can be similar to those caused by changing the force field. This was shown by Zhang et al.[33] who studied the same systems as Hanus and Mazeau[24] in vacuum and in explicit water. Mazeau and Charlier found also that the geometrical features of the adsorption with and without explicitly accounting for water were very similar. Studies dealing with solvation in aqueous solvents must, however, be done with explicit water to account for the entropy contributions of adsorbed water molecules that are released into the water bulk. Such studies were performed for example by Bergenstråhle et al.[25,34] When force fields are used, the implicit quantum nature of the carbohydrate system is neglected; the quality of such a description cannot be discerned from the parametrization process, because many of the commonly used potentials (e.g., GLYCAM06[35]) have not been designed for the description of surface adsorption. A small number of studies was performed with quantum theoretical methods; studies where the role of dispersion is explicitly accounted for are more reliable than older studies, where dispersion was neglected. Kubicki et al.[36] studied water adsorption with density functional theory (DFT) and empirical dispersion correction, Bourassa et al.[37] investigated the role of sodium cations on the adsorption of water on cellulose using MP2 and DFT with empirical dispersion corrections, and Li et al.[38] investigated the crystal structure of cellulose Iα and Iβ with dispersion corrected DFT and stressed the importance of dispersion for both the crystal structure and the adsorption of water. Stabilization energies reported in these studies are purely electronic energies.

In this work, we study the adsorption of glucose, cellobiose, and cellotetraose onto clean (100) surfaces of cellulose Iα and Iβ. These surfaces were chosen because in a previous study on the adsorption of water onto cellulose[39] we could show that not only strongly exposed oxygen groups, causing the hydrophilicity of the surface, have a strong influence on the strength of interaction with the water molecules but also the different morphology, mainly the roughness, of this surface enhances the

dx.doi.org/10.1021/jp5025685 | J. Phys. Chem. B 2014, 118, 9017−9027

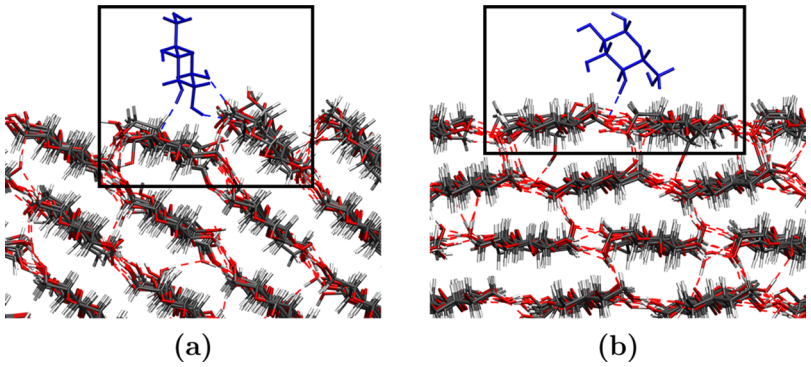

Figure 1. Schematic view of the adsorption of glucose on a cellulose Iα (100) (a) and a Iβ (100) surface (b). The surface model systems used in this work are displayed in the black rectangles.

interaction with the adsorbed molecules. In the Iα (100) system the bulk sheets are not parallel to the surface, in the layers parallel to the surface the glucose rings are slanted and the free hydroxyl groups at the edges are strongly exposed. This surface is hydrophilic. In the flat Iβ (100) surface the bulk sheets are parallel to the surface, there are no free hydroxyl groups, most of them are involved in interchain hydrogen bonds and thus cannot be easily accessed by adsorbates. This surface is strongly hydrophobic.[19] We investigate the adsorption of water-free small carbohydrates from the gas phase on water-free cellulose surfaces, a situation that is experimentally nearly impossible to realize but is compatible with bad solvent conditions. An important issue of this work is validation of the quality of the GLYCAM06 force field by comparison with DFT and dispersion-corrected DFT for the adsorption of a single glucose molecule. We find that GLYCAM06 provides accurate equilibrium geometries and, in most cases, accurate adsorption energies. Another issue of this work is to find out how the size of the adsorbate determines the dominant interaction type, that is, when dispersion becomes more important than hydrogen bonding. Because of the good agreement between force field and DFT data, we study the adsorption of cellobiose and cellotetraose using the GLYCAM06 force field only.

Three important findings of our work are, first, adsorption on cellulose Iα (100) is, in general, stronger than adsorption on cellulose Iβ (100); second, the nature of the surface becomes less important with increasing adsorbate size; and third, the adsorption energy is not directly proportional to the number of hydrogen bonds and, moreover, dispersion interactions must be taken into account for a correct description of the adsorption.

METHODS

The model systems for both surface types, namely cellulose Iα (100) and cellulose Iβ (100) surfaces, consist of small cutouts (strands) of a pair of adjacent glucan molecules of different lengths. For the adsorption of glucose we used two cellobiose strands as model surfaces; for the adsorption of cellobiose and cellotetraose we used surface models made of two cellooctaose strands to accommodate the larger adsorbate molecules. In the following, these model structures are referred to as "surfaces". The size of the model surfaces enables us to capture the major contribution of the top layer to surface adsorption, while neglecting the much smaller contributions from lower-lying bulk layers and from neighboring surface strands. The surface models were constructed from optimized and equilibrated surface slabs that were generated in a previous study[39] employing the GLYCAM06[35] force field. In Figure 1, the surface models are shown within these slabs.

To get a reliable sample of structures for which the interaction energy is calculated, we chose trial geometries for the optimization in the following way: Adsorbates with more than one glucose ring were regarded as flat ribbons, so that we can clearly distinguish between a growth direction or molecular axis corresponding to the principle axis of inertia associated with the smallest moment of inertia, the 1-axis, and a molecular geometry plane normal to the principle axis of inertia corresponding to the largest moment of inertia, the 3-axis. The adsorbate was first positioned parallel to the surface on top of one glucan strand, and the shortest distances between carbon atoms were chosen to be about 4 Å; then the adsorbate was translated along the growth direction of the glucan strand by half of the length of one glucose ring. A second set of trial geometries was obtained by placing the adsorbate between the glucan strands and modifying the geometries as before. Further trial geometries were obtained by rotating around the 3-axis in steps of 45° so that the molecular axes of the adsorbate and the growth direction of the surface were no longer parallel. The last set of trial geometries was obtained by rotating the adsorbate by 45° and 90° about the molecular axis and again translating it along the growth direction of the glucan strands.

For glucose the axis going through the exocyclic hydroxymethyl group was chosen as the molecular axis and translation was performed as described for the larger adsorbates. Additional positions were constructed by rotating planar glucose about the 2-axis in steps of 45°, so that the hydroxymethyl group was either closest to or most distant from the surface. Again, the shortest C−C distances were about 4 Å. This procedure was applied to get trial geometries for the adsorbates on both the Iα and the Iβ surfaces.

The geometries of the surface/glucose complexes were optimized using the BP86[40,41] functional together with the def2-SVP basis set,[42] starting from the trial geometries described above. All atoms of the surface models were kept frozen during optimization, except for the OH groups and the exocyclic hydroxymethyl groups. All optimizations were performed with the package TURBOMOLE[43−46] using the resolution of the identity approximation.[47−52] Default convergence criteria for electronic structure and geometry were used. Geometry optimizations yielded structures that can be classified as parallel or vertical according to a parameter γ, which is the angle between the principal axis of the glucose molecule corresponding to the largest principal moment of inertia and the surface plane. Details can be found in the

dx.doi.org/10.1021/jp5025685 | J. Phys. Chem. B 2014, 118, 9017−9027

Supporting Information. For each surface two vertical and one parallel structure were chosen as representatives, in the first vertical structure the glucose is positioned on top of one glucan chain and in the second it is positioned between the two glucan chains. To estimate the influence of dispersion interactions on cellulose surface adsorption, the BP86-optimized representatives were reoptimized by employing an additional empirical dispersion correction, namely, the D2 scheme, as described by Grimme,[53] giving the BP86-D2-optimized structures.

To find out how well the BP86-D2 results agree with the GLYCAM06 force field used in the surface equilibration, the BP86-D2-optimized structures were reoptimized with the GLYCAM06 force field,[35] yielding the GLYCAM06-optimized structures. All force field calculations were performed with DL_POLY[54] using the ChemShell 3.3.1 interface[55] and the geometry optimizer DL-FIND.[56] Input files were generated by using AmberTools 1.4[57] with the GLYCAM06g parameters. The geometry was edited with the model builder Aten[58] and visualized with VMD.[59]

The adsorption energy E_{ads} for adsorption on the crystal surface was calculated with the following expression:

$$E_{ads} = E_{surface} + E_{adsorbate} - E_{surface+adsorbate} \quad (1)$$

and using the methods BP86, BP86-D2, B3LYP,[40,60,61] B3LYP-D2,[53] B3LYP-D3,[62,63] M06-2X,[64] ωB97X-D,[65,66] and GLYCAM06.[35] M06-2X is a highly parametrized density functional that is capable of describing medium-range dispersion effects.

The five methods BP86-D2, B3LYP-D2, B3LYP-D3, ωB97X-D, and M06-2X, which cover medium or long-range dispersion are termed DFT-D methods; the two methods BP86 and B3LYP will be referred to as DFT methods throughout this paper. For all DFT and DFT-D adsorption-energy calculations, the counterpoise (CP) correction was applied.[67]

The M06-2X and ωB97X-D calculations were performed with Gaussian 09[68] by using the def2-TZVP basis set; for all other DFT and DFT-D calculations we used TURBOMOLE,[44−46] the def2-TZVP basis set, the resolution of the identity approximation with the corresponding auxiliary basis set,[47−52] and default settings on electronic structure convergence.

Adsorption energies calculated with BP86/def2-TZVP and BP86/def2-QZVP differed by only 0.1 kJ/mol (or 0.2%); therefore, the def2-TZVP basis set was deemed sufficient for the calculation of this observable. The corresponding convergence test was made for a single surface/glucose structure.

Due to the immense computational expense of the larger systems, the adsorption of cellobiose and cellotetraose was only studied with the GLYCAM06 force field. The number and selection of the systems used are described below.

The naming convention for the atoms in a glucose unit is shown in Figure 2. In this work, hydrogen bonds are defined as O−H···O moieties, in which the first oxygen atom belongs always to the adsorbate, irrespective of being a donor or acceptor atom. Only hydrogen bonds between the surface and the adsorbed molecules will be discussed. For a detailed discussion of intrasurface hydrogen bonds see Maurer et al.[39]

RESULTS AND DISCUSSION

Adsorption of β-D-Glucose. The six BP86-optimized geometries (blue) along with the corresponding BP86-D2-optimized geometries (red) and GLYCAM06-optimized geometries (green) are shown in Figure 3.

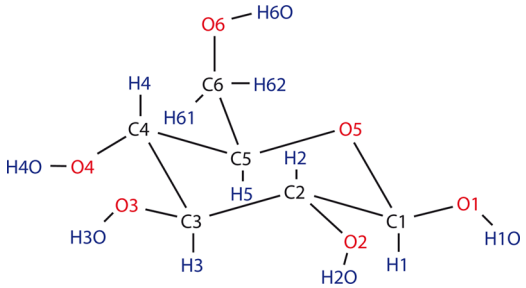

Figure 2. Naming convention employed for atoms within a glucose molecule.

For comparison of the optimized structures we use the following information: the angle γ (described above), the normal distance *d* between the centers of mass of the surface and the glucose molecule, the root-mean-square distance (RMSD) between two structures, and hydrogen bonds. All γ, *d*, and RMSD values are given in the Supporting Information. Because BP86-D2 is expected to give the most reliable results only differences with respect to this method are discussed in the following. For γ the ranges of the deviations from BP86-D2 are −20.0 to +25.1° for BP86 and −35.0 to +8.0° for GLYCAM06, the mean of the absolute values is 9.2° and 10.5°, respectively. Except for one structure, GLYCAM06 and BP86 yield larger values of *d* than BP86-D2, the exception is the GLYCAM06-optimized structure Iα-1. The ranges of the deviations from BP86-D2 are 0.12−0.46 Å for BP86 and −0.33 to +0.41 Å for GLYCAM06, the means of the absolute values are 0.29 and 0.26 Å, respectively. The ranges of the RMSD values are 0.09−0.77 Å for BP86 and 0.18−0.73 Å for GLYCAM06; the means are 0.42 and 0.43 Å, respectively. These three parameters show that structures obtained with all three methods are remarkably similar.

Finally, we can use the occurrence or absence of hydrogen bonds between surface and adsorbate to compare the optimized structures. In Figure 3 only hydrogen bonds with an O−O distance below 3.5 Å and an O−H···O angle greater than 140° are shown. In Iα-1, optimized with BP86 and BP86-D2, there are three hydrogen bonds (O1−H···O3, O1···H−O2, and O6−H···O3), whereas in the GLYCAM06 optimized structure, the O6−H···O3 hydrogen bond is missing. The parallel Iα-2 structure contains only one hydrogen bond (O6···H−O2) according to all optimization methods. In Iα-3, all methods find two hydrogen bonds (O2−H···O6 and O1···H−O2); BP86-D2 finds also an O3−H···O4 hydrogen bond.

For Iβ-1, the three methods are not in agreement: With BP86 there are three hydrogen bonds (O3−H···O3, O4−H···O5, and O4···H−O1), with BP86-D2 we find two hydrogen bonds (O3−H···O3 and O4−H···O5), and with GLYCAM06 there is only one hydrogen bond (O3−H···O3). For the parallel Iβ-2 structure there is, however, good agreement among all methods. The parallel orientation of the glucose rings does not allow any hydrogen bonds to be formed with the surface, which is also the case between layers of cellulose strands in the cellulose Iβ crystal.[39,69] All methods also agree for Iβ-3, predicting only one hydrogen bond (O4−H···O6).

The importance of dispersion interactions for accurately predicting the adsorption structure can be seen when complexes with weakly interacting molecules are optimized, such as the parallel Iα-2 model: starting from a structure in which the glucose is aligned parallel and relatively far away from the surface, no attractive interactions are described by BP86,

dx.doi.org/10.1021/jp5025685 | J. Phys. Chem. B 2014, 118, 9017−9027

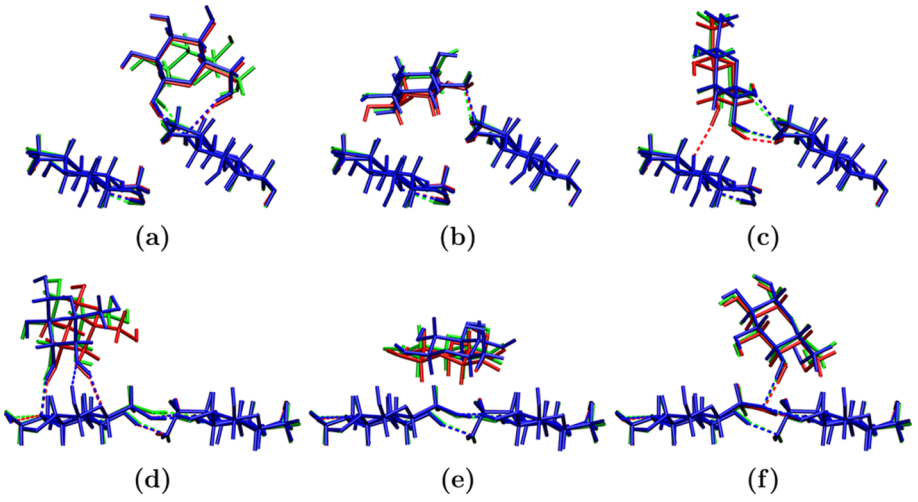

Figure 3. Optimized structures of glucose on the model surfaces for systems Iα-1 (a), Iα-2 (b), Iα-3 (c), Iβ-1 (d), Iβ-2 (e), and Iβ-3 (f) calculated with BP86 (blue), BP86-D2 (red), and GLYCAM06 (green). The view direction is the growth direction of the surface glucan chains.

and the starting geometry is not changed. In contrast, with BP86-D2 and GLYCAM06, the glucose molecule is pulled toward the surface and hydrogen bonds are formed (Figure 4).

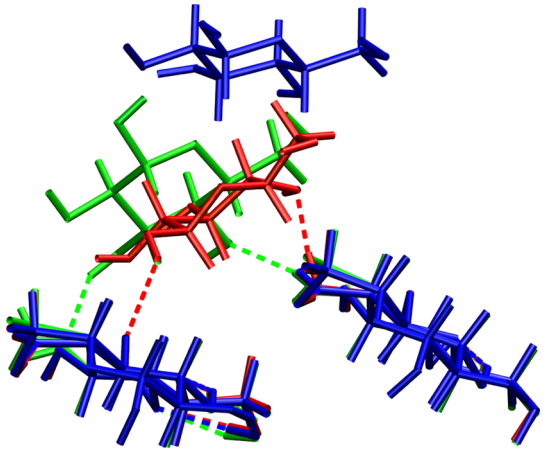

Figure 4. Effect of dispersion interactions: Final optimized geometries via methods with and without van-der-Waals terms. BP86 (blue), BP86-D2 (red), GLYCAM06 (green). The starting geometry is always the same and it is nearly identical to the BP86 optimized geometry.

Adsorption Energies for BP86-Optimized Structures. We calculated the adsorption energies with all previously mentioned methods for the geometries optimized with BP86, BP86-D2, and GLYCAM06. We start with the discussion of the adsorption energies for the BP86-optimized structures (Figure 5 and Table S1 of the Supporting Information).

As can be inferred from Figure 5, the BP86 and B3LYP adsorption energies are nearly identical, and roughly half of the DFT-D values. One can also see that the CP-corrected DFT adsorption energies for Iβ-2 are very small and negative, and therefore repulsive. M06-2X yields the lowest and B3LYP-D2 the highest DFT-D values; the values differ by between 11 and 19 kJ/mol. GLYCAM06 values are surprisingly close to the DFT-D values.

The DFT-D methods yield very similar trends for the different structures, whereas the GLYCAM06 energies sometimes over- and sometimes undershoot the DFT-D adsorption energies. We find fair agreement between the GLYCAM06 and

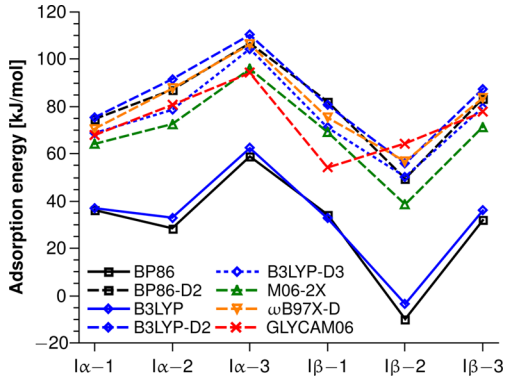

Figure 5. Adsorption energies for the BP86-optimized structures.

DFT-D values for the Iα structures, whereas for the Iβ structures there are larger differences: for structure Iβ-1, the GLYCAM06 value is smaller than the DFT-D values, but for structure Iβ-2 it is larger. The BP86-optimized structure Iβ-1 has three hydrogen bonds; for this structure, GLYCAM06 yields a poor interaction energy. On the other hand, Iβ-2 has no hydrogen bonds at all and the GLYCAM06 adsorption energy is larger than all the DFT-D values.

For every structure, we calculated the mean value of the DFT-D adsorption energies $\bar{E}_{\text{DFT-D}}$ with corresponding standard deviation (σ), the difference between the GLYCAM06 value and the DFT-D mean value $E_{\text{FF}} - \bar{E}_{\text{DFT-D}}$, and the maximal difference between DFT-D values $\Delta_{\text{max}}E_{\text{DFT-D}}$ (Table 1).

There is good agreement for the Iα structures between the GLYCAM06 data and the corresponding mean values of the DFT-D data $\bar{E}_{\text{DFT-D}}$, the absolute values of $E_{\text{FF}} - \bar{E}_{\text{DFT-D}}$ are smaller than the corresponding values of $\Delta_{\text{max}}E_{\text{DFT-D}}$. For the I$\beta$ structures, GLYCAM06 values give no systematic error when compared to the respective DFT-D mean values. The absolute value of $E_{\text{FF}} - \bar{E}_{\text{DFT-D}}$ can be larger than the maximal difference among the DFT-D values.

Adsorption Energies for BP86-D2-Optimized Structures. The adsorption energies for the BP86-D2-optimized structures are shown in Figure 6 and in Table S2 of the Supporting Information. In Table 2, mean DFT-D values, GLYCAM06 values, and deviations are listed.

dx.doi.org/10.1021/jp5025685 | J. Phys. Chem. B 2014, 118, 9017−9027

Table 1. Statistics of the Adsorption Energies for the BP86-Optimized Structures[a]

structure	$\bar{E}_{\text{DFT-D}} \pm \sigma$	E_{FF}	$E_{\text{FF}} - \bar{E}_{\text{DFT-D}}$	$\Delta_{\max}E_{\text{DFT-D}}$
Iα-1	70.8 ± 4.6	67.9	−2.9	11.2
Iα-2	83.5 ± 7.7	80.7	−2.8	19.0
Iα-3	104.7 ± 5.4	94.2	−10.5	14.4
Iβ-1	75.7 ± 5.7	54.2	−21.5	12.9
Iβ-2	50.2 ± 7.2	64.4	14.2	18.1
Iβ-3	81.1 ± 6.1	77.7	−3.4	16.1

[a]Shown are the mean values of the DFT-D adsorption energies ($\bar{E}_{\text{DFT-D}}$) with standard deviations (σ), GLYCAM06 adsorption energies (E_{FF}), the differences between the GLYCAM06 values and the mean DFT-D values ($E_{\text{FF}} - \bar{E}_{\text{DFT-D}}$), and the maximal differences between DFT-D values ($\Delta_{\max}E_{\text{DFT-D}}$). All energies are in kJ/mol.

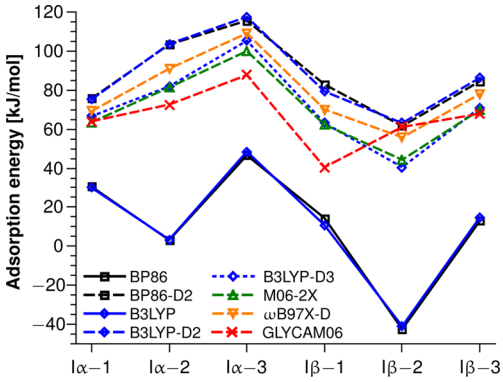

Figure 6. Adsorption energies for the BP86-D2-optimized structures.

Table 2. Statistics of the Adsorption Energies for the BP86-D2-Optimized Structures[a]

structure	$\bar{E}_{\text{DFT-D}} \pm \sigma$	E_{FF}	$E_{\text{FF}} - \bar{E}_{\text{DFT-D}}$	$\Delta_{\max}E_{\text{DFT-D}}$
Iα-1	70.0 ± 5.3	64.0	−6.0	12.2
Iα-2	92.3 ± 11.0	72.6	−19.7	22.3
Iα-3	109.5 ± 7.2	87.7	−21.8	17.5
Iβ-1	71.5 ± 9.3	40.5	−31.0	20.6
Iβ-2	53.1 ± 10.2	61.2	8.1	22.6
Iβ-3	77.9 ± 7.6	67.9	−10.0	16.5

[a]Shown are the mean values of the DFT-D adsorption energies ($\bar{E}_{\text{DFT-D}}$) with standard deviations (σ), GLYCAM06 adsorption energies (E_{FF}), the differences between the GLYCAM06 values and the mean DFT-D values ($E_{\text{FF}} - \bar{E}_{\text{DFT-D}}$), and the maximal differences between DFT-D values ($\Delta_{\max}E_{\text{DFT-D}}$). All energies are in kJ/mol.

DFT adsorption energies for BP86-D2-optimized structures are always considerably smaller than for the BP86-optimized structures; the parallel structure Iβ-2 is destabilized by about 40 kJ/mol, whereas structure Iα-2 is nearly unbound. The fact that all BP86-D2 adsorption energies for BP86-D2-optimized structures are larger than for the BP86-optimized structures is not surprising. For the other DFT-D methods the same is not generally true. Indeed, we find a larger spread of adsorption energies ($\Delta_{\max}E_{\text{DFT-D}}$) for all BP86-D2-optimized structures than what was found for the BP86-optimized structures.

The GLYCAM06 adsorption energies are smaller than the mean DFT-D values for all but one structure; the exception is again the hydrogen-bond-free structure Iβ-2, in which the GLYCAM06 value is nearly as large as the largest DFT-D value. The lowest of all GLYCAM06 adsorption energies is found for the hydrogen-bonded structure Iβ-1. A comparison of the DFT-D and GLYCAM06 values shows that, for the BP86-D2-optimized structures, the differences between $\bar{E}_{\text{DFT-D}}$ and the corresponding GLYCAM06 values are mostly larger than for the BP86-optimized structures; for two structures, the absolute values of $E_{\text{FF}} - \bar{E}_{\text{DFT-D}}$ are even larger than $\Delta_{\max}E_{\text{DFT-D}}$ (Table 2). Nevertheless, the agreement between GLYCAM06 results and the DFT-D mean values is quite remarkable.

Adsorption Energies for GLYCAM06-Optimized Structures. The adsorption energies for the GLYCAM06-optimized structures are shown in Figure 7 and in Table S3 of the Supporting Information; mean DFT-D values, GLYCAM06 values, and deviations are listed in Table 3.

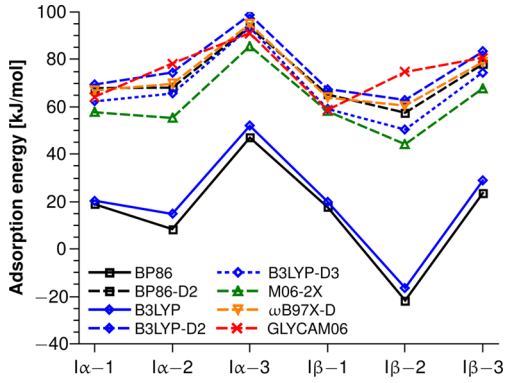

Figure 7. Adsorption energies for the GLYCAM06-optimized structures.

Table 3. Statistics of the Adsorption Energies for the GLYCAM06-Optimized Structures[a]

structure	$\bar{E}_{\text{DFT-D}} \pm \sigma$	E_{FF}	$E_{\text{FF}} - \bar{E}_{\text{DFT-D}}$	$\Delta_{\max}E_{\text{DFT-D}}$
Iα-1	64.8 ± 4.8	64.2	−0.6	11.7
Iα-2	66.6 ± 7.1	78.3	11.7	19.2
Iα-3	93.3 ± 4.8	91.1	−2.2	13.2
Iβ-1	62.8 ± 4.0	58.7	−4.1	9.4
Iβ-2	55.1 ± 7.7	74.7	19.6	18.7
Iβ-3	76.6 ± 5.8	80.7	4.2	15.5

[a]Shown are the mean values of the DFT-D adsorption energies ($\bar{E}_{\text{DFT-D}}$) with standard deviations (σ), GLYCAM06 adsorption energies (E_{FF}), the differences between the GLYCAM06 values and the mean DFT-D values ($E_{\text{FF}} - \bar{E}_{\text{DFT-D}}$), and the maximal differences between DFT-D values ($\Delta_{\max}E_{\text{DFT-D}}$). All energies are in kJ/mol.

Again, the lowest adsorption energies are obtained with the DFT methods. Structure Iβ-2 is found to be unstable by about 20 kJ/mol. A remarkably good agreement between GLYCAM06 and DFT-D adsorption energies is found for the vertical structures; the absolute values of $E_{\text{FF}} - \bar{E}_{\text{DFT-D}}$ are all less than 5 kJ/mol, and much lower than $\Delta_{\max}E_{\text{DFT-D}}$. For both parallel structures, however, the GLYCAM06 values are larger than the largest DFT-D values. Compared with the BP86-D2-optimized structures, all GLYCAM06 adsorption energies are, on average, larger by 3 kJ/mol for the Iα structures and by 15 kJ/mol for the Iβ structures.

Method Comparison. As already discussed, the optimized structures obtained with BP86, BP86-D2, and GLYCAM06 are generally quite similar. The largest differences between the optimized structures are found for structures Iα-1 and Iβ-1, where the glucose molecule is vertically positioned above one glucan chain; for the other four structures, the agreement between the three methods is quite remarkable. However, the

dx.doi.org/10.1021/jp5025685 | J. Phys. Chem. B 2014, 118, 9017−9027

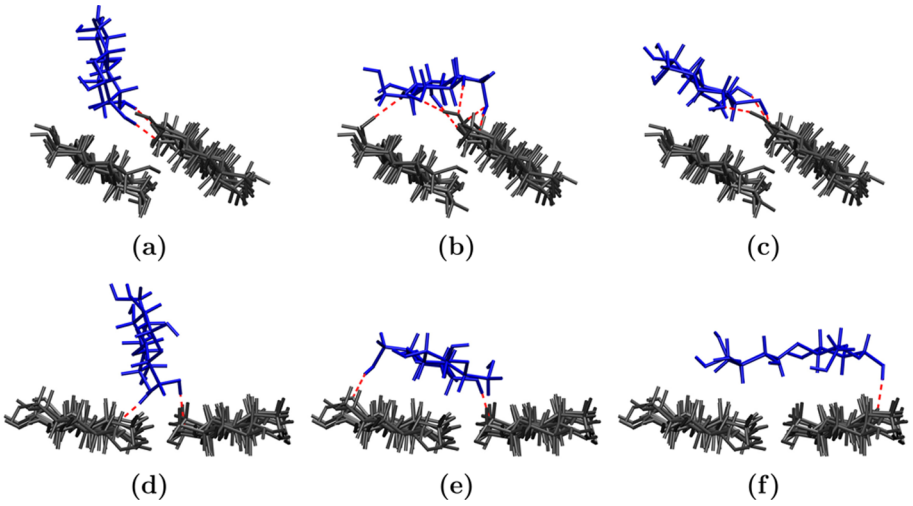

Figure 8. Representative geometries of the cellobiose adsorption: Iα-vertical (a), Iα-parallel (b), Iα-diagonal (c), Iβ-vertical (d), Iβ-parallel (e), Iβ-parallel, and orthogonal (f).

good agreement between BP86 and BP86-D2-optimized geometries is only observed when in the starting geometries for the BP86 optimizations the adsorbate and the model surface are already close to each other; otherwise, BP86 optimizations yield wrong structures because of the missing attractive dispersion forces. Except for Iα-1, BP86-D2 optimizations yield the shortest distances between adsorbate and surface (Table S5 in the Supporting Information).

The agreement is all the more remarkable considering that two very different theoretical methods are used to describe the noncovalent interactions between the adsorbate and the surface model. In both cases, the potential energy surfaces can be very flat with respect to intermolecular coordinates. A full account of dispersion interactions is essential for a correct description of the adsorption geometry, which is the case for almost all generally used force field approaches including GLYCAM06. The good agreement between the structures optimized with BP86 and the other two methods was due to the chosen trial geometries; if the distance between the adsorbate and the surface is larger than 5 Å, DFT without dispersion correction is not able to produce reliable geometries.

Considering adsorption energies, the observed differences between the methods are larger. Comparison of the adsorption energies at the three sets of optimized structures (Tables 1−3) shows that DFT adsorption energies are only a fraction of the DFT-D and GLYCAM06 adsorption energies. At least half of the adsorption energy is due to the dispersion correction. GLYCAM06 and DFT-D energies agree for Iα structures better than for Iβ structures. When the absolute adsorption energy for a given structure is investigated (Figures 5−7), the agreement between GLYCAM06 and the mean DFT-D adsorption energy is, in general, better than the agreement among the various DFT-D methods.

All DFT-D methods yield the same relative order of energies among various geometries; the Iα-3 complex is predicted to be the most stable, and the Iβ-2 complex to be the least stable. GLYCAM06, on the other hand, does not yield the same order of energies. Compared to DFT-D energies, adsorption energies of structures exhibiting a large number of hydrogen bonds are slightly underestimated (cf. structure Iβ-1 in Figures 5−7); for structures with no hydrogen bonds, GLYCAM06 adsorption energies are systematically overestimated. This effect is particularly evident for rigid small molecules with adsorption geometries that are mainly dispersion bound. In the case of large flexible adsorbates that can easily form hydrogen bonds, such as medium-chain carbohydrates, this effect should be less pronounced.

In summary, GLYCAM06 gives an overall good description of adsorption geometries and energetics. Therefore, GLYCAM06 can safely be used to study the adsorption of medium-sized flexible carbohydrate-based adsorbates that are used for functionalizing cellulose surfaces. In the following, we will investigate the adsorption of cellobiose and cellotetraose on our model surfaces to estimate the dependency of the adsorption geometry and energy on the adsorbate size.

Adsorption of Cellobiose. From the large number of stable surface/cellobiose structures, 43 were selected and divided into 6 different groups according to the alignment of the cellobiose on the surface. Among the 17 structures obtained for the cellulose Iα surface, we distinguish by visual inspection between vertical, parallel, and diagonal structures, the latter look as if they were at an intermediate stage in crystal growth. This classification is supported by structural parameters that are given and explained in the Supporting Information.

The 26 structures adsorbed to the cellulose Iβ surface were grouped into vertical and two differently aligned parallel structures. A different number of stable structures was included in each group. In parallel structures, cellobiose molecules can include any angle with the glucan molecules of the surface; nevertheless, we only investigated structures in which the growth directions of the cellobiose molecule and the glucan molecules are aligned or orthogonal to each other. One representative of each group is shown in Figure 8. Pictures and adsorption energies of all members of each group can be found in the Supporting Information. Mean values, standard deviations, and the highest calculated adsorption energy for each group are listed in Table 4.

On both surfaces we find higher adsorption energies for parallel structures than for nonparallel structures, because there are more atom pairs in close contact in parallel structures than in nonparallel structures; thus, the loss of dispersion energy in the latter structures cannot be compensated by hydrogen bonds.

dx.doi.org/10.1021/jp5025685 | J. Phys. Chem. B 2014, 118, 9017−9027

Table 4. GLYCAM06 Mean Adsorption Energies of Cellobiose (Maximal Values in Parentheses) in kJ/mol

adsorbate orientation	Iα	Iβ
vertical	155 ± 20 (178)	99 ± 17 (114)
parallel	209 ± 32 (238)	139 ± 32 (186)
parallel, orthogonal		120 ± 14 (141)
diagonal	180 ± 23 (206)	

The mean energy for the adsorption of a cellobiose molecule onto the cellulose Iα surface is 185 ± 35 kJ/mol (calculated for 17 structures); for adsorption onto the cellulose Iβ surface, it is 120 ± 28 kJ/mol (calculated for 26 structures).

One reason for the strong adsorption to cellulose Iα is certainly the larger number of hydrogen bonds that can be formed, because on cellulose Iα more oxygen atoms are accessible to the adsorbate than on cellulose Iβ. For cellulose Iα, the highest observed number of hydrogen bonds between the cellobiose and the surface model is 6, but for cellulose Iβ, it is only 2. Because of the grooved shape of the Iα surface, small molecules can generally get closer to the surface than they can in Iβ (Figure 9).

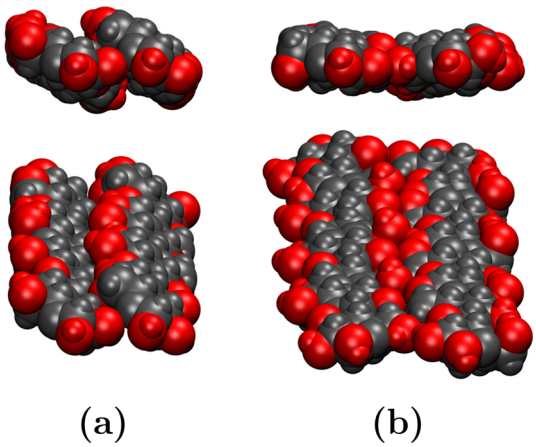

Figure 9. Parallel glucan molecules as model systems for the cellulose Iα(100) surface (a) and the cellulose Iβ(100) surface (b).

Adsorption of Cellotetraose. For the adsorption of cellotetraose 14 Iα structures and 18 Iβ structures were divided into groups of vertical, parallel, and twisted structures; for cellulose Iα, we also investigated one diagonal structure. A detailed description of this classification is given in the Supporting Information.

Again, different numbers of stable structures of each type were found and sorted into the various groups. The number of stable parallel structures is much larger than the number of either vertical or twisted structures. In Figure 10, only representatives of those groups that were not found among the cellobiose structures are shown. Pictures and adsorption energies of all members of each group can be found in the Supporting Information. In Table 5, the mean values, standard deviations, and the highest calculated adsorption energies for each group are listed.

The highest adsorption energies for both cellulose surfaces were found for parallel adsorption; the differences between adsorption energies of vertical and twisted structures are rather small. The crystal-growth-like structure (diagonal) has one of the largest adsorption energies.

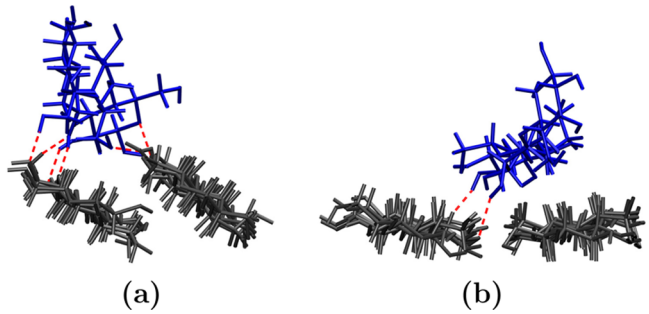

Figure 10. Representative geometries of the cellotetraose adsorption: Iα-twisted (a) and Iβ-twisted (b). Only orientations that were not observed in the cellobiose adsorption are shown.

Table 5. GLYCAM06 Mean Adsorption Energies of Cellotetraose (Maximal Values in Parentheses) in kJ/mol

adsorbate orientation	Iα	Iβ
vertical	249 ± 35 (289)	189 ± 31 (214)
parallel	325 ± 32 (374)	290 ± 20 (325)
twisted	231 ± 24 (251)	211 ± 27 (247)
diagonal	342	

The mean energy for the adsorption of a cellotetraose molecule onto the cellulose Iα surface is 289 ± 53 kJ/mol (calculated for 14 structures); for adsorption onto the cellulose Iβ surface, it is 255 ± 50 kJ/mol (calculated for 18 structures).

Discussion of the Carbohydrate Adsorption. Comparison of all adsorption energies shows that adsorption onto the more hydrophilic cellulose Iα surface is stronger than onto the cellulose Iβ surface; however, the difference becomes smaller with increasing size of the adsorbate. This can also be clearly seen from the adsorption energy per glucose residue in the adsorbate (see below).

The highest adsorption energies are always observed when the glucose residues are parallel to the surface, because the number of adsorbate atoms that are in close contact with the surface atoms is maximized in this orientation, and this leads to high adsorption energies due to the large dispersion contributions. On the contrary, for vertical structures, the number of hydrogen bonds is maximized but at the cost of a tremendous loss of dispersion energy, which cannot be compensated by the larger number of hydrogen bonds. With increasing size of the adsorbate, the energy difference between parallel and nonparallel alignment with the glucan molecules vanishes; for small adsorbates, parallel alignment is preferred to nonparallel alignment with the glucan molecules.

We do not observe any direct correlation between the adsorption energy and the number of intermolecular hydrogen bonds in the complex, as can be demonstrated by the Iβ/cellobiose structures: The structure shown in Figure S6 (g) of the Supporting Information (glucose rings parallel to the surface, the cellobiose molecule orthogonal to the glucan chain) has no hydrogen bonds and an adsorption energy of 127 kJ/mol; the structure with the highest adsorption energy of 186 kJ/mol has two hydrogen bonds. The difference between the highest and lowest adsorption energy for structures with no hydrogen bond is 38 kJ/mol; for structures with one hydrogen bond the difference is 100 kJ/mol, whereas for structures with two hydrogen bonds it is 109 kJ/mol. These differences are mainly due to the different dispersion interactions in these complexes.

dx.doi.org/10.1021/jp5025685 | J. Phys. Chem. B 2014, 118, 9017−9027

That the dispersion contributions become more important for larger adsorbates can be seen from the mean adsorption energies per glucose residue: for cellobiose, it is 93 kJ/mol on the hydrophilic Iα surface and 60 kJ/mol on the hydrophobic Iβ surface; for the larger cellotetraose, the values are 72 and 64 kJ/mol, respectively. We see that, with increasing size of the adsorbate, the adsorption energies become more similar, regardless of surface hydrophilicity. Averaging over the Iα and the Iβ values yields 77 kJ/mol for cellobiose and 68 kJ/mol for cellotetraose; this suggests that an adsorption energy between 70 and 75 kJ/mol could be a reasonable estimate for the adsorption energy per glucose residue for oligosaccharides on any kind of cellulose I surface.

The geometry data for glucose, the smallest adsorbate in this study, do not fit this trend because, for this small molecule, vertical structures with hydrogen bonds are more favorable than for the large adsorbates, in which dispersion is more important than hydrogen bonding. The mean adsorption energies (calculated for the three selected structures) are 78 kJ/mol for the Iα surface and 71 kJ/mol for the Iβ surface; if we take the average, we get a mean value of 75 kJ/mol, which is compatible with the estimate.

CONCLUSION

We investigated the adsorption of a glucose molecule on models of the (100) surfaces of crystalline cellulose Iα and Iβ with the GLYCAM06 force field, the BP86 density functional, and BP86-D2, using an empirical dispersion correction. We find that GLYCAM06 yields geometries that are in good agreement with the BP86-D2 results. Comparison of adsorption energies calculated with GLYCAM06 and all DFT-D methods for the GLYCAM06 optimized structures shows surprisingly good agreement for all structures with hydrogen bonds; the adsorption energy for structures with very few hydrogen bonds, however, is overestimated by GLYCAM06 by up to about 30%. We assume that this effect is much smaller for larger adsorbates that are more flexible around the glycosidic bond and therefore able to form more hydrogen bonds. All adsorption energies obtained with density functional theory methods that do not account for dispersion interactions are completely at odds with the DFT-D and GLYCAM06 data; in fact, GLYCAM06 describes all our structures better than the DFT methods. This shows, once more, that inclusion of dispersion interactions is essential for accurate description of molecular structure and energetics.

Employing GLYCAM06 for investigating the adsorption of larger analogues of glucose, namely, cellobiose and cellotetraose, we found that the adsorption energy increased with the size of the adsorbate, but we found no direct correlation with the number of intermolecular hydrogen bonds in the complexes. Nevertheless, with the increasing size of the adsorbate, the hydrophilicity of the cellulose surface becomes less important. This is consistent with the increasing relevance of dispersion interactions in stabilizing the complex. We have given a rough estimate of the adsorption energy per glucose residue for cellulose surfaces regardless of surface hydrophilicity. More reliable adsorption energies, as well as quality assessments of dynamical observables such as charge reordering and solubility, can be obtained by using explicit dynamics simulations with the GLYCAM06 force field.

Attractive hydrophobic interaction, that is, dispersion interaction, becomes important the larger the interacting systems are, because dispersion is nearly isotropic and thus largely independent of the relative orientation. The only relevant factor is that the sum of interatomic distances gets minimal. This was shown by Hoja et al.[23] recently. Dispersion is ubiquitous, it is also a major component in hydrogen bonds, which are traditionally thought to be stabilized by anisotropic dipole−dipole interactions. If hydrogen bonding were the dominant component in the adsorption of large carbohydrates on cellulose, one should find a pronounced correlation of stabilization with the number of connecting O−H···O groups, which we do not find. Our findings are, however, compatible with the model for crystal growth of cellulose by Cousins and Brown.[70] These authors proposed as initial step formation of dispersion stabilized stacks of glucan molecules, in a second step these stacks interact via their hydrophilic side faces so that interchain hydrogen bonds can be formed. One could, therefore, compare the stabilizing interactions in cellulose with reinforced concrete, where isotropic dispersion plays the role of concrete and hydrogen bonds act like rebars that support, but do not dominate, bonding. This view of the role of hydrogen bonding is compatible with O'Sullivan's description according to which intrachain hydrogen bonds "may act to determine the "straightness" of the chain. Interchain hydrogen bonds might introduce order or disorder into the system, depending on its regularity".[1] Dissolution of cellulose is according to this bonding model not a process where spatially localized hydrogen bonds must be broken, but where nonlocalized dispersion dominated hydrophobic attraction must be destroyed. Our results clearly support the Lindman hypothesis.[16]

ASSOCIATED CONTENT

Supporting Information

All adsorption energies and structural parameters for all surface/adsorbate structures, pictures of all surface/cellobiose and surface/cellotetraose complexes, and the complete Gaussian 09 reference are presented in the Supporting Information. This material is available free of charge via the Internet at http://pubs.acs.org/.

AUTHOR INFORMATION

Corresponding Author

*A. Sax. E-mail: alexander.sax@uni-graz.at.

Notes

The authors declare no competing financial interest.

ACKNOWLEDGMENTS

The authors acknowledge financial support by the European Union Seventh Framework Program project SURFUNCELL, Grant agreement No. 214653. Helpful comments and suggestions by the reviewers are gratefully acknowledged.

REFERENCES

(1) O'Sullivan, A. Cellulose: The Structure Slowly Unravels. *Cellulose* **1997**, *4*, 173−207.

(2) Nogi, M.; Iwamoto, S.; Nakagaito, A. N.; Yano, H. Optically Transparent Nanofiber Paper. *Adv. Mater.* **2009**, *21*, 1595−1598.

(3) Raghavendra, G. M.; Jayaramudu, T.; Varaprasad, K.; Sadiku, R.; Ray, S. S.; Raju, K. M. Cellulose-Polymer-Ag Nanocomposite Fibers for Antibacterial Fabrics/Skin Scaffolds. *Carbohydr. Polym.* **2013**, *93*, 553−560.

(4) Okahisa, Y.; Yoshida, A.; Miyaguchi, S.; Yano, H. Optically Transparent Wood-Cellulose Nanocomposite as a Base Substrate for

Flexible Organic Light-Emitting Diode Displays. *Compos. Sci. Technol.* **2009**, *69*, 1958−1961.
(5) Findenig, G.; Leimgruber, S.; Kargl, R.; Spirk, S.; Stana-Kleinschek, K.; Ribitsch, V. Creating Water Vapor Barrier Coatings from Hydrophilic Components. *ACS Appl. Mater. Interfaces* **2012**, *4*, 3199−3206.
(6) Medronho, B.; Romano, A.; Miguel, M. G.; Stigsson, L.; Lindman, B. Rationalizing Cellulose (In)solubility: Reviewing Basic Physicochemical Aspects and Role of Hydrophobic Interactions. *Cellulose* **2012**, *19*, 581−587.
(7) Medronho, B.; Lindman, B. Competing Forces During Cellulose Dissolution: From Solvents to Mechanisms. *Curr. Opin. Colloid Interface Sci.* **2014**, *19*, 32−40.
(8) Nishiyama, Y.; Sugiyama, J.; Chanzy, H.; Langan, P. Crystal Structure and Hydrogen Bonding System in Cellulose Iα from Synchrotron X-Ray and Neutron Fiber Diffraction. *J. Am. Chem. Soc.* **2003**, *125*, 14300−14306.
(9) Nishiyama, Y.; Langan, P.; Chanzy, H. Crystal Structure and Hydrogen-Bonding System in Cellulose Iβ from Synchrotron X-Ray and Neutron Fiber Diffraction. *J. Am. Chem. Soc.* **2002**, *124*, 9074−9082.
(10) Shen, T.; Gnanakaran, S. The Stability of Cellulose: A Statistical Perspective from a Coarse-Grained Model of Hydrogen-Bond Networks. *Biophys. J.* **2009**, *96*, 3032−3040.
(11) Nishiyama, Y.; Johnson, G. P.; French, A. D.; Forsyth, V. T.; Langan, P. Neutron Crystallography, Molecular Dynamics, and Quantum Mechanics Studies of the Nature of Hydrogen Bonding in Cellulose Iβ. *Biomacromolecules* **2008**, *9*, 3133−3140.
(12) Qian, X.; Ding, S.-y.; Nimlos, M. R.; Johnson, D. K.; Himmel, M. E. Atomic and Electronic Structures of Molecular Crystalline Cellulose Iβ: A First-Principles Investigation. *Macromolecules* **2005**, *38*, 10580−10589.
(13) Lindman, B.; Karlström, G.; Stigsson, L. On the Mechanism of Dissolution of Cellulose. *J. Mol. Liq.* **2010**, *156*, 76−81.
(14) Bodvik, R.; Dedinaite, A.; Karlson, L.; Bergstrom, M.; Baverback, P.; Pedersen, J.; Edwards, K.; Karlsson, G.; Varga, I.; Claesson, P. Aggregation and Network Formation of Aqueous Methylcellulose and Hydroxypropylmethylcellulose Solutions. *Colloids Surf., A* **2010**, *354*, 162−171.
(15) Zhang, L.; Ruan, D.; Gao, S. Dissolution and Regeneration of Cellulose in NaOH/Thiourea Aqueous Solution. *J. Polym. Sci., Part B: Polym. Phys.* **2002**, *40*, 1521−1529.
(16) Glasser, W. G.; Atalla, R. H.; Blackwell, J.; Malcolm Brown, R.; Burchard, W.; French, A. D.; Klemm, D. O.; Nishiyama, Y. About the Structure of Cellulose: Debating the Lindman Hypothesis. *Cellulose* **2012**, *19*, 589−598.
(17) Isobe, N.; Noguchi, K.; Nishiyama, Y.; Kimura, S.; Wada, M.; Kuga, S. Role of Urea in Alkaline Dissolution of Cellulose. *Cellulose* **2013**, *20*, 97−103.
(18) Xiong, B.; Zhao, P.; Hu, K.; Zhang, L.; Cheng, G. Dissolution of Cellulose in Aqueous NaOH/Urea Solution: Role of Urea. *Cellulose* **2014**, *21*, 1183−1192.
(19) Mazeau, K.; Rivet, A. Wetting the (110) and (100) Surfaces of Iβ Cellulose Studied by Molecular Dynamics. *Biomacromolecules* **2008**, *9*, 1352−1354.
(20) Himmel, M. E.; Ding, S.-Y.; Johnson, D. K.; Adney, W. S.; Nimlos, M. R.; Brady, J. W.; Foust, T. D. Biomass Recalcitrance: Engineering Plants and Enzymes for Biofuels Production. *Science* **2007**, *315*, 804−807.
(21) Stone, A. *The Theory of Intermolecular Forces*, 2nd ed.; Oxford Press: Oxford, U.K., 2013.
(22) Jeffrey, G. A. *An Introduction to Hydrogen Bonding*; Oxford University Press: New York, 1997.
(23) Hoja, J.; Sax, A. F.; Szalewicz, K. Is Electrostatics Sufficient to Describe Hydrogen-Bonding Interactions? *Chem. - Eur. J.* **2014**, *20*, 2292−2300.
(24) Hanus, J.; Mazeau, K. The Xyloglucan-Cellulose Assembly at the Atomic Scale. *Biopolymers* **2006**, *82*, 59−73.
(25) Bergenstråhle, M.; Wohlert, J.; Himmel, M. E.; Brady, J. W. Simulation Studies of the Insolubility of Cellulose. *Carbohydr. Res.* **2010**, *345*, 2060−2066.
(26) Mazeau, K.; Charlier, L. The Molecular Basis of the Adsorption of Xylans on Cellulose Surface. *Cellulose* **2012**, *19*, 337−349.
(27) Peri, S.; Muthukumar, L.; Nazmul Karim, M.; Khare, R. Dynamics of Cello-Oligosaccharides on a Cellulose Crystal Surface. *Cellulose* **2012**, *19*, 1791−1806.
(28) Zhao, Z.; Crespi, V. H.; Kubicki, J. D.; Cosgrove, D. J.; Zhong, L. Molecular Dynamics Simulation Study of Xyloglucan Adsorption on Cellulose Surfaces: Effects of Surface Hydrophobicity and Side-Chain Variation. *Cellulose* **2014**, *21*, 1025−1039.
(29) Mazeau, K.; Vergelati, C. Atomistic Modeling of the Adsorption of Benzophenone onto Cellulosic Surfaces. *Langmuir* **2002**, *18*, 1919−1927.
(30) Mazeau, K.; Wyszomirski, M. Modelling of Congo Red Adsorption on the Hydrophobic Surface of Cellulose Using Molecular Dynamics. *Cellulose* **2012**, *19*, 1495−1506.
(31) Nimlos, M. R.; Beckham, G. T.; Matthews, J. F.; Bu, L.; Himmel, M. E.; Crowley, M. F. Binding Preferences, Surface Attachment, Diffusivity, and Orientation of a Family 1 Carbohydrate-Binding Module on Cellulose. *J. Biol. Chem.* **2012**, *287*, 20603−20612.
(32) Nypelö, T.; Pynnönen, H.; Österberg, M.; Paltakari, J.; Laine, J. Interactions Between Inorganic Nanoparticles and Cellulose Nanofibrils. *Cellulose* **2012**, *19*, 779−792.
(33) Zhang, Q.; Brumer, H.; Ågren, H.; Tu, Y. The Adsorption of Xyloglucan on Cellulose: Effects of Explicit Water and Side Chain Variation. *Carbohydr. Res.* **2011**, *346*, 2595−2602.
(34) Bergenstråhle, M.; Wohlert, J.; Larsson, P. T.; Berglund, L. A.; Mazeau, K. Dynamics of Cellulose-Water Interfaces: NMR Spin-Lattice Relaxation Times Calculated from Atomistic Computer Simulations. *J. Phys. Chem. B* **2008**, *112*, 2590−2595.
(35) Kirschner, K. N.; Yongye, A. B.; Tschampel, S. M.; González-Outeiriño, J.; Daniels, C. R.; Foley, B. L.; Woods, R. J. GLYCAM06: A Generalizable Biomolecular Force Field. Carbohydrates. *J. Comput. Chem.* **2008**, *29*, 622−655.
(36) Kubicki, J. D.; Watts, H. D.; Zhao, Z.; Zhong, L. Quantum Mechanical Calculations on Cellulose-Water Interactions: Structures, Energetics, Vibrational Frequencies and NMR Chemical Shifts for Surfaces of Iα and Iβ Cellulose. *Cellulose* **2014**, *21*, 909−926.
(37) Bourassa, P.; Bouchard, J.; Robert, S. Quantum Chemical Calculations of Pristine and Modified Crystalline Cellulose Surfaces: Benchmarking Interactions and Adsorption of Water and Electrolyte. *Cellulose* **2014**, *21*, 71−86.
(38) Li, Y.; Lin, M.; Davenport, J. W. Ab Initio Studies of Cellulose I: Crystal Structure, Intermolecular Forces, and Interactions with Water. *J. Phys. Chem. C* **2011**, *115*, 11533−11539.
(39) Maurer, R. J.; Sax, A. F.; Ribitsch, V. Molecular Simulation of Surface Reorganization and Wetting in Crystalline Cellulose I and II. *Cellulose* **2013**, *20*, 25−42.
(40) Becke, A. D. Density-Functional Exchange-Energy Approximation with Correct Asymptotic Behavior. *Phys. Rev. A* **1988**, *38*, 3098−3100.
(41) Perdew, J. Density-Functional Approximation for the Correlation Energy of the Inhomogeneous Electron Gas. *Phys. Rev. B* **1986**, *33*, 8822−8824.
(42) Schäfer, A.; Horn, H.; Ahlrichs, R. Fully Optimized Contracted Gaussian Basis Sets for Atoms Li to Kr. *J. Chem. Phys.* **1992**, *97*, 2571.
(43) *TURBOMOLE* V6.3 2011, A Development of University of Karlsruhe and Forschungszentrum Karlsruhe GmbH, 1989−2007, TURBOMOLE GmbH, since 2007; available from http://www.turbomole.com.
(44) Ahlrichs, R.; Bär, M.; Häser, M.; Horn, H.; Kölmel, C. Electronic Structure Calculations on Workstation Computers: The Program System Turbomole. *Chem. Phys. Lett.* **1989**, *162*, 165−169.
(45) Treutler, O.; Ahlrichs, R. Efficient Molecular Numerical Integration Schemes. *J. Chem. Phys.* **1995**, *102*, 346.

(46) Von Arnim, M.; Ahlrichs, R. Performance of Parallel TURBOMOLE for Density Functional Calculations. *J. Comput. Chem.* **1998**, *19*, 1746−1757.
(47) Eichkorn, K.; Treutler, O.; Öhm, H.; Häser, M.; Ahlrichs, R. Auxiliary Basis Sets to Approximate Coulomb Potentials. *Chem. Phys. Lett.* **1995**, *240*, 283−290.
(48) Eichkorn, K.; Treutler, O.; Öhm, H.; Häser, M.; Ahlrichs, R. Auxiliary Basis Sets to Approximate Coulomb Potentials (Chem. Phys. Letters 240 (1995) 283−290). *Chem. Phys. Lett.* **1995**, *242*, 652−660.
(49) Eichkorn, K.; Weigend, F.; Treutler, O.; Ahlrichs, R. Auxiliary Basis Sets for Main Row Atoms and Transition Metals and Their Use to Approximate Coulomb Potentials. *Theor. Chem. Acc.* **1997**, *97*, 119−124.
(50) Weigend, F. Accurate Coulomb-Fitting Basis Sets for H to Rn. *Phys. Chem. Chem. Phys.* **2006**, *8*, 1057−1065.
(51) Weigend, F. A Fully Direct RI-HF Algorithm: Implementation, Optimised Auxiliary Basis Sets, Demonstration of Accuracy and Efficiency. *Phys. Chem. Chem. Phys.* **2002**, *4*, 4285−4291.
(52) Armbruster, M. K.; Weigend, F.; van Wüllen, C.; Klopper, W. Self-Consistent Treatment of Spin-Orbit Interactions with Efficient Hartree-Fock and Density Functional Methods. *Phys. Chem. Chem. Phys.* **2008**, *10*, 1748−1756.
(53) Grimme, S. Semiempirical GGA-Type Density Functional Constructed with a Long-Range Dispersion Correction. *J. Comput. Chem.* **2006**, *27*, 1787−1799.
(54) Smith, W. The DL_POLY Molecular Simulation Package, CSE Department, *STFC Daresbury Laboratory*.
(55) *ChemShell*, a Computational Chemistry Shell, see www.chemshell.org.
(56) Kästner, J.; Carr, J. M.; Keal, T. W.; Thiel, W.; Wander, A.; Sherwood, P. DL-FIND: An Open-Source Geometry Optimizer for Atomistic Simulations. *J. Phys. Chem. A* **2009**, *113*, 11856−11865.
(57) Case, D. A.; Darden, T. A.; Cheatham, T. E.; Simmerling, C. L.; Wang, J.; Duke, R. E.; Luo, R.; Crowley, M.; Walker, R. C.; Zhang, W.; et al. *Amber 11*; University of California: San Francisco, 2008.
(58) Youngs, T. G. A. Aten-An Application for the Creation, Editing, and Visualization of Coordinates for Glasses, Liquids, Crystals, and Molecules. *J. Comput. Chem.* **2010**, *31*, 639−648.
(59) Humphrey, W.; Dalke, A.; Schulten, K. VMD: Visual Molecular Dynamics. *J. Mol. Graph.* **1996**, *14*, 33−38.
(60) Lee, C.; Yang, W.; Parr, R. G. Development of the Colle-Salvetti Correlation-Energy Formula into a Functional of the Electron Density. *Phys. Rev. B* **1988**, *37*, 785−789.
(61) Becke, A. D. Density-Functional Thermochemistry. III. The Role of Exact Exchange. *J. Chem. Phys.* **1993**, *98*, 5648−5652.
(62) Grimme, S.; Antony, J.; Ehrlich, S.; Krieg, H. A Consistent and Accurate Ab Initio Parametrization of Density Functional Dispersion Correction (DFT-D) for the 94 Elements H-Pu. *J. Chem. Phys.* **2010**, *132*, 154104.
(63) Grimme, S.; Ehrlich, S.; Goerigk, L. Effect of the Damping Function in Dispersion Corrected Density Functional Theory. *J. Comput. Chem.* **2011**, *32*, 1456−1465.
(64) Zhao, Y.; Truhlar, D. G. The M06 Suite of Density Functionals for Main Group Thermochemistry, Thermochemical Kinetics, Noncovalent Interactions, Excited States, and Transition Elements: Two New Functionals and Systematic Testing of Four M06-Class Functionals and 12 Other Functionals. *Theor. Chem. Acc.* **2008**, *120*, 215−241.
(65) Chai, J.-D.; Head-Gordon, M. Systematic Optimization of Long-Range Corrected Hybrid Density Functionals. *J. Chem. Phys.* **2008**, *128*, 084106.
(66) Chai, J.-D.; Head-Gordon, M. Long-Range Corrected Hybrid Density Functionals with Damped Atom-Atom Dispersion Corrections. *Phys. Chem. Chem. Phys.* **2008**, *10*, 6615−6620.
(67) Boys, S.; Bernardi, F. The Calculation of Small Molecular Interactions by the Differences of Separate Total Energies. Some Procedures with Reduced Errors. *Mol. Phys.* **1970**, *19*, 553−566.
(68) Frisch, M. J.; Trucks, G. W.; Schlegel, H. B.; Scuseria, G. E.; Robb, M. A.; Cheeseman, J. R.; Scalmani, G.; Barone, V.; Mennucci, B.; Petersson, G. A.; et al. *Gaussian 09*, Revision A.02; Gaussian Inc.: Wallingford, CT, 2009.
(69) Matthews, J. F.; Skopec, C. E.; Mason, P. E.; Zuccato, P.; Torget, R. W.; Sugiyama, J.; Himmel, M. E.; Brady, J. W. Computer Simulation Studies of Microcrystalline Cellulose Iβ. *Carbohydr. Res.* **2006**, *341*, 138−152.
(70) Cousins, S. K.; Brown, R. Cellulose I Microfibril Assembly: Computational Molecular Mechanics Energy Analysis Favours Bonding by Van Der Waals Forces as the Initial Step in Crystallization. *Polymer* **1995**, *36*, 3885−3888.